# A mathematical model of metacarpal subchondral bone adaptation, microdamage, and repair in racehorses

Michael Pan[1,2,3], Fatemeh Malekipour[4], Peter Pivonka[5], Ashleigh V Morrice-West[1], Jennifer A Flegg[2,3], R Chris Whitton[1], Peta L Hitchens[1]*

[1]Equine Centre, Melbourne Veterinary School, Faculty of Science, The University of Melbourne, Werribee, VIC 3030, Australia
[2]School of Mathematics and Statistics, The University of Melbourne, Parkville 3010, Victoria, Australia
[3]ARC Centre of Excellence for the Mathematical Analysis of Cellular Systems, University of Melbourne, Parkville, Victoria 3010, Australia
[4]Department of Biomedical Engineering, University of Melbourne, Parkville, VIC 3010, Australia
[5]School of Mechanical, Medical and Process Engineering, Queensland University of Technology, Brisbane, QLD 4000, Australia

*Corresponding author: peta.hitchens@unimelb.edu.au

**Abstract**

Fractures of the distal limb in Thoroughbred racehorses primarily occur because of accumulation of bone microdamage from high-intensity training. Mathematical models of subchondral bone adaptation of the third metacarpal lateral condyles are capable of approximating existing data for Thoroughbred racehorses in training or at rest. To improve upon previous models, we added a dynamic resorption rate and microdamage accumulation and repair processes. Our ordinary differential equation model simulates the coupled processes of bone adaptation and microdamage accumulation, and is calibrated to data on racehorses in training and rest. Sensitivity analyses of our model suggest that joint loads and distances covered per day are among the most significant parameters for predicting microdamage accumulated during training. We also use the model to compare the impact of incremental increasing training programs as horses enter training from a period of rest and maintenance workloads of horses that are race fit on bone adaptation. We find that high-speed training accounts for the majority of damage to the bone. Furthermore, for horses in race training, the estimated rates of bone repair are unable to offset the rate of damage accumulation under a typical Australian racing campaign, highlighting the need for regular rest from training.

## Nomenclature

| Symbol | Description | Units |
|---|---|---|
| $f_{BM}$ | Bone volume fraction | – |
| $S_v$ | Bone specific surface | $\mathrm{mm}^{-1}$ |
| $D^*$ | Bone damage | – |
| $X$ | Number of microcracks | – |
| $E$ | Bone stiffness | MPa |
| $\sigma$ | Joint contact pressure | MPa |
| $\psi$ | Strain energy density | MPa |
| $\dot{\varepsilon}$ | Strain rate | $\mathrm{s}^{-1}$ |
| $v_n$ | Number of cycles per day | $\mathrm{day}^{-1}$ |
| $N_f$ | Fatigue life | – |
| $\alpha$ | Fraction of surface available for remodelling | – |
| $E_0$ | Maximum bone stiffness | MPa |
| $A_{\mathrm{OBL}}$ | Bone formation rate | mm/day |
| $A_{\mathrm{OCL}}$ | Bone resorption rate | mm/day |
| $F_s$ | Damage repair specificity factor | – |

# 1 Introduction

Bone fractures are a major concern in Thoroughbred racehorses, with the subchondral bone of the distal third metacarpal bone being a common site of injury [1–3]. To achieve fitness and musculoskeletal adaptation to race conditions, mechanical loading is primarily introduced via repeated cyclical loading (strides) at incrementally increasing speeds. However, too many cycles at high-intensity loads may be injurious [4–6]. Previous epidemiological studies have found both the speed and distances worked during training to be linked to bone fractures and musculoskeletal injury [6, 7]. However, training can also have a protective effect on bone, with cumulative gallop distances over a career being linked to lower fracture incidence rates [6]. These conflicting findings of both too little and too much high-speed exercise associated with catastrophic musculoskeletal injury [8] highlight the importance of understanding the biological process of bone adaptation, damage accumulation and repair.

Mathematical models of bone adaptation due to mechanical loading have a long history in development and have provided many insights into the fundamental mechanisms playing roles in bone adaptation [9, 10]. In the context of exercise controlled bone adaptation responses in humans two major computational modeling themes have emerged: (i) models for predicting stress fractures in athletes and soldiers [11, 12] and (ii) enhancement of drug efficacy with exercise for osteoporosis treatments [13, 14]. Both of these modeling approaches require linking of the mechanostat feedback with bone damage accumulation and repair during high cyclic loading and rest intervals, respectively. There have been several modelling studies on bone adaptation and damage in the trabecular and cortical bone of humans [12, 15–17].

While the above-described models of coupled bone adaptation, damage accumulation and repair have been applied to human studies, to the authors' knowledge, no such models exist for Thoroughbred racehorses. A previous model of subchondral bone adaptation in the third metacarpal bone in Thoroughbred racehorses predicted changes in bone volume fraction ($f_{BM}$) with joint stress [18]. Morrice-West et al. [19] subsequently developed a method for calculating

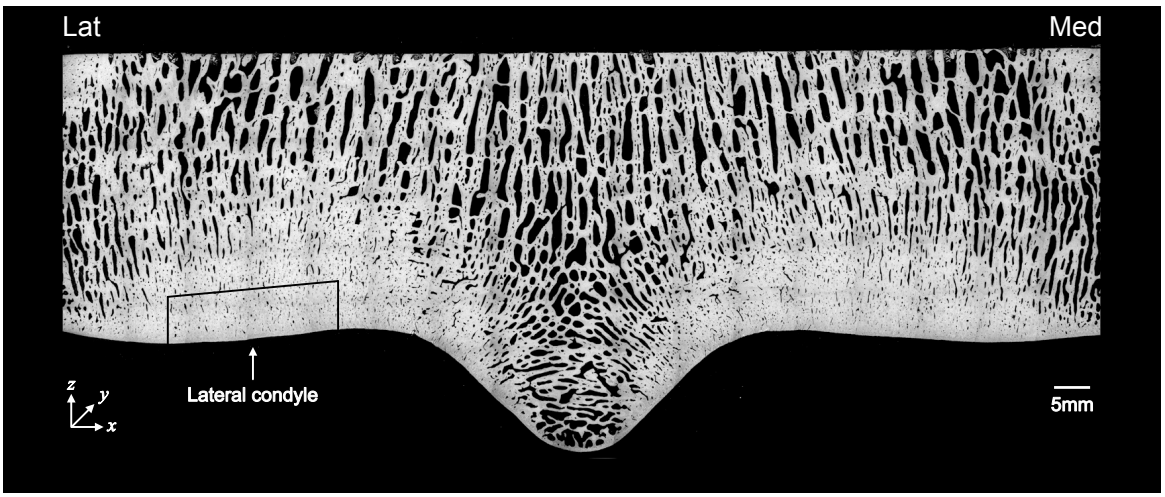


**Figure 1:** Back-scattered electron microscopy image of the distal third metacarpal bone in a Thoroughbred racehorse. The volume of interest is the mid lateral condyle articular margin, indicated by the arrow. The coordinate system is defined as $x$, mediolateral; $y$, dorsodistal $z$, distopalmar direction. Adapted with permission from Holmes et al. [24].

bone damage accumulated using experimentally derived relationships between stress and bone fatigue life [20].

Here, we aim to extend our previous model of subchondral bone adaptation in the third metacarpal bone in Thoroughbred racehorses [18] to incorporate bone damage accumulation and repair processes. In particular, we add a dynamic resorption rate which depends on loading intensity and differential equations accounting for bone microdamage accumulation and repair. The resorption rate of the third metacarpal (MCIII) condyles is generally higher than the bone formation rate except at the highest levels of mechanical loading [21–23]. Hitchens et al. [18] modelled bone resorption as a constant rate, however, osteoclastic resorption is inhibited by intense race training [24, 25]. The rate of bone damage accumulation increases exponentially with the magnitude of load [19, 20], and we use this relationship to model damage formation in our model. Furthermore, we derive equations for bone repair that are coupled to the dynamics of bone formation and resorption following the approach of Martin [15] and Hazelwood et al. [26].

In this study, we aim to develop a computational model of bone adaptation for Thoroughbred racehorses, including damage accumulation and repair. We calibrate the model to measurements from horses resting and in race training, and simulate the response of bone to a typical training program based on surveyed workloads of racehorses in Vitcoria, Australia [27]. We hypothesise that (i) the joint stress and number of cycles (strides) per day are key determinants of bone injury risk; (ii) training programs with greater volumes of high-speed gallops are more likely to lead to bone injuries; and (iii) rest periods are essential to bone repair. This extended model will help us to enhance understanding of the processes of bone adaptation, microdamage accumulation, and repair to the subchondral bone of the distal metacarpus of racehorses, forming the basis for assessing and developing safer training strategies that reduce the risk of racehorse injury.

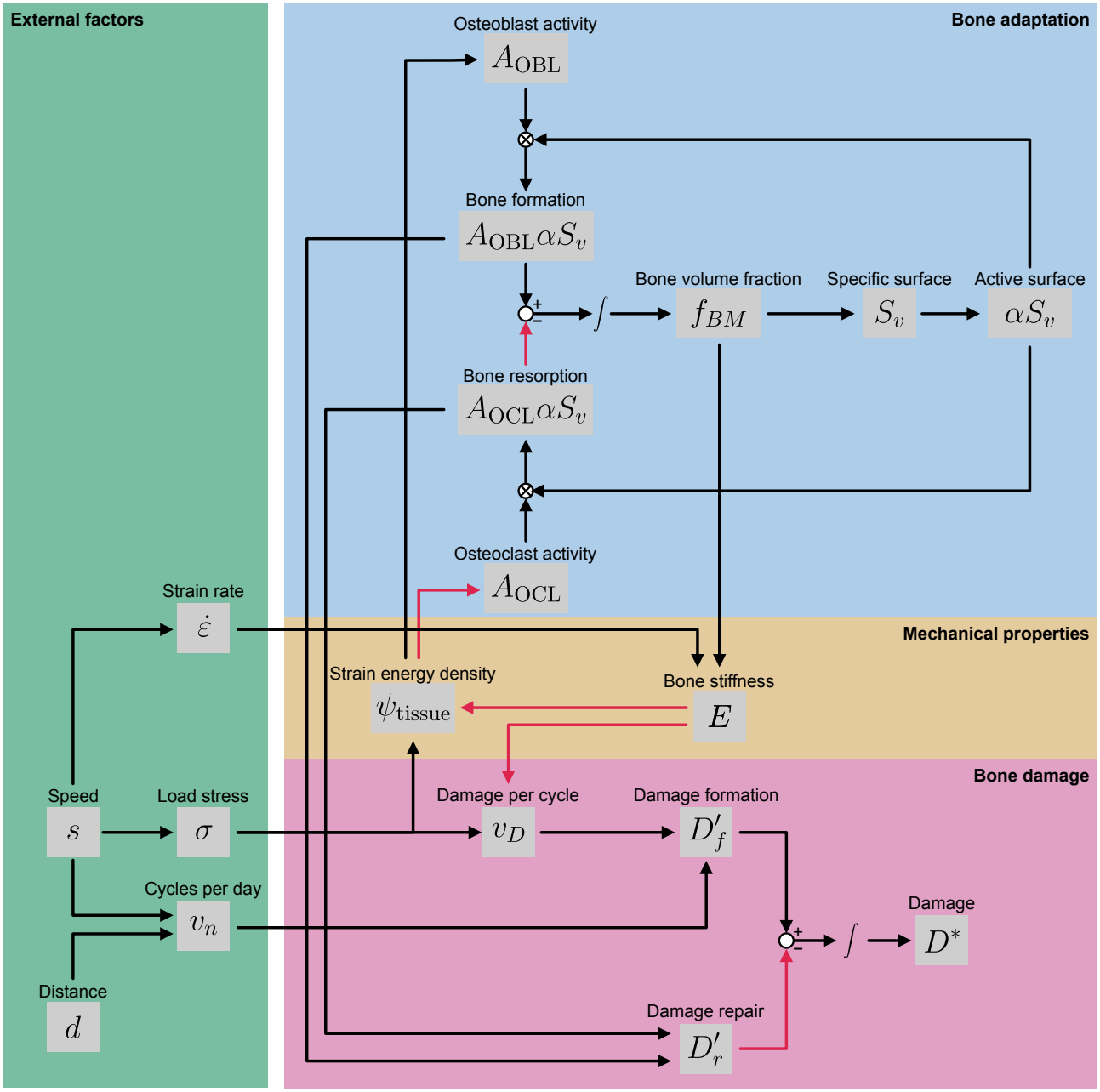


**Figure 2:** Schematic of the bone adaptation and damage model. Activating relationships are shown by black arrows, and inhibitory relationships are shown by red arrows. (Blue box) The subchondral bone consists of regions of bone matrix and empty regions of marrow. Remodelling occurs at the interface of bone and marrow. On average, the surface area ($S_v$) available for remodelling decreases with increasing bone volume fraction ($f_{\mathrm{BM}}$). Osteoblasts (with activity $A_{\mathrm{OBL}}$) are responsible for bone formation, whereas osteoclasts (with activity $A_{\mathrm{OCL}}$) are responsible for bone resorption. (Yellow box) The bone senses mechanical stresses through its strain energy density $\psi_{\mathrm{tissue}}$, which acts as a signal for bone adaptation. (Pink box) Stresses incurred on the bone lead to the accumulation of damage ($D^*$) through microcracks. These microcracks can be removed through osteoclast resorption. (Green box) The speeds ($s$) and distances ($d$) of training programs correspond to both bone stress ($\sigma$) and number of cycles ($v_n$) [28], inducing bone formation but also causing microdamage. Open circles indicate the addition or subtraction of variables, and circles with crosses inside indicate multiplication.

## 2 Methods

In this section, we describe our model of bone adaptation and damage within a region of interest at the lateral condyle of the third metacarpal bone (Figure 1). The model is defined by Eqs (1)–(12). A summary of the processes modelled is schematically shown in Figure 2.

### 2.1 Base mathematical model of bone adaptation

The base model of subchondral bone adaptation of the equine distal metacarpus is described in detail in Hitchens et al. [18]. The model consists of an ordinary differential equation (ODE) described by two main equations

$$S_v = a\sqrt{1 - f_{BM}} \cdot [1 - b(1 - f_{BM})], \tag{1}$$

$$\frac{df_{BM}}{dt} = (A_{\text{OBL}} - A_{\text{OCL}})\alpha S_v. \tag{2}$$

Eq. (1) is a function that expresses the relationship between the bone volume fraction $f_{BM}$ [dimensionless] and bone specific surface $S_v$ [mm$^{-1}$] (Figure 2; blue box). This equation is the square root function previously derived by Lerebours et al. [29], with parameters modified to fit bone data from racehorses ($a = 11.42$ mm$^{-1}$ and $b = -0.02$). Eq. (2) is a mass balance of the bone volume fraction [30] (Figure 2; blue box). $A_{\text{OBL}}$ [mm/day] is the bone formation activity (bone volume change per unit time per unit surface area), and $A_{\text{OCL}}$ [mm/day] is the bone resorption activity. In Hitchens et al. [18], $A_{\text{OBL}}$ is dynamic and dependent on strain energy density $\psi_{\text{tissue}}$ [MPa], whereas $A_{\text{OCL}}$ was assumed constant. However, as explained later in Subsection 2.2, we use dynamic resorption rates for both activities, and update the equations for both $A_{\text{OBL}}$ and $A_{\text{OCL}}$. The rates of bone formation and resorption are both proportional to $\alpha$, the specific surface available for bone remodelling. It is assumed that bone properties are homogeneous throughout the metacarpal condyles.

The model also assumes that osteocytes sense mechanical forces through the strain energy density $\psi_{\text{tissue}}$, which in turn affects the osteoblast activity $A_{\text{OBL}}$ (Figure 2; yellow box). Supposing there is a uniaxial linear constitutive relationship between the stress-states $\sigma$ [MPa] and strain $\varepsilon$, the strain energy density is given by

$$\psi_{\text{tissue}} = \frac{1}{2E}\sigma^2, \tag{3}$$

where $E$ [MPa] is the tissue stiffness [18]. The loading state is assumed to be uniaxial, i.e. $\sigma = \sigma_{zz}$ and $\sigma_{xx} = \sigma_{yy} = \sigma_{xy} = \sigma_{xz} = \sigma_{yz} = 0$ (coordinates indicated in Figure 1). Since bone stiffness has been observed to increase with both bone density and strain rate, the tissue stiffness is set to

$$E = E_0 \dot{\varepsilon}^{\gamma_E} f_{BM}^3 \tag{4}$$

with $\gamma_E = 0.06$, as described previously [18].

### 2.2 Extended mathematical model of bone adaptation

The base model is updated to incorporate the effects of $\psi_{\text{tissue}}$ on both the bone formation activity $A_{\text{OBL}}$ and resorption activity $A_{\text{OCL}}$ (Figure 2; blue box). Osteocytes in the bone tissue are mechanosensors, that is, they are assumed to sense a mechanical load in the form of strain energy density. These osteocytes release biochemical signals that affect bone formation and

resorption rates. Bone formation rates are higher in unadapted bone subjected to high-speed exercise [21, 23]. This is modelled using the Hill equation

$$A_{\mathrm{OBL}} = A_{\mathrm{OBL}}^{\min} + \frac{(A_{\mathrm{OBL}}^{\max} - A_{\mathrm{OBL}}^{\min})\psi_{\mathrm{tissue}}^{\gamma_B}}{(\delta_B^{\gamma_B} + \psi_{\mathrm{tissue}}^{\gamma_B})}, \tag{5}$$

where $A_{\mathrm{OBL}}^{\min}$ [mm/day] is the minimum bone formation rate, $A_{\mathrm{OBL}}^{\max}$ [mm/day] is the maximum bone formation rate, $\delta_B$ [MPa] is the half-saturation constant and $\gamma_B$ [dimensionless] is the sigmoidicity.

Conversely, high-speed exercise inhibits bone resorption [24, 31, 32]. Thus, the bone resorption rate decreases when bone is subjected to higher loads. This is modelled using the decreasing Hill function

$$A_{\mathrm{OCL}} = A_{\mathrm{OCL}}^{\min} + \frac{(A_{\mathrm{OCL}}^{\max} - A_{\mathrm{OCL}}^{\min})\delta_C^{\gamma_C}}{(\delta_C^{\gamma_C} + \psi_{\mathrm{tissue}}^{\gamma_C})}, \tag{6}$$

with constants defined similarly to Eq. (5). We set the minimum resorption rate to 0.001 mm/day [33], and assume that $\gamma_C = 2$ to achieve a sigmoidal relationship. Horses at rest have been observed to have four times the erosion surface of horses in full training, which translates to higher resorption rates [24]. We thus tune this equation by selecting a proxy for rest at a load of 30 MPa, and for race-fit training and racing at 90 MPa. Using the corresponding stiffnesses for a horse that has been adapted to racing speeds and distances at $f_{BM} = 0.9$ (see Table 3 of Hitchens et al. [18]), these stresses correspond to strain energy densities of 0.31 and 2.36 respectively. We therefore set the half-saturation constant to $\delta_C = 1.0$ MPa so that bone resorption is activated in between the two loads. While the maximum resorption rate $A_{\mathrm{OCL}}^{\max}$ is estimated to be as high as 0.011 mm/day in untrained two-year-old horses [33], we believe this is an overestimate as it results in excessive bone resorption within our model. Thus, we fit this parameter to time-series data on bone volume fractions (Subsection A.3, electronic supplementary material). The curves for $A_{\mathrm{OBL}}$ and $A_{\mathrm{OCL}}$ (after fitting) as functions of $\psi_{\mathrm{tissue}}$ are shown in Figure S8 of the electronic supplementary material.

## 2.3 Bone microdamage

It is widely accepted that the majority of equine bone injuries occur due to bone fatigue, the gradual accumulation of microcracks in the bone until a fracture occurs. Microdamage accumulation as a result of cyclical loading is non-linear, typically occurring in three stages. In a study of racehorses, most subchondral bone specimens under compressive fatigue increased stiffness rapidly in the initial stage, then plateaued during the mid-stages close to or at maximum stiffness, then in the final stage decreased rapidly to failure [20]. Less commonly, in specimens with shorter fatigue life, either stiffness decreased sharply between the initial stage and the plateau phase or a steady decrease in stiffness replaced the plateau stage [20]. The reason for the plateau in stiffness and strength is due to build up of residual strain. Eventually, the microcracks propagate and overwhelm the bone repair process until catastrophic failure [34]. The loads experienced by the subchondral bone of the distal third metacarpal bone within Thoroughbred racehorses are predominantly compressive [35], leading to microcracks oriented obliquely to the articular surface [36].

Carter and Caler [37] used the framework of continuum damage mechanics to develop a mathematical model which linked load and bone damage. Subsequently, several researchers expanded upon this model [12, 15, 38]. While there are multiple definitions of damage in the literature [13, 15, 39, 39–42], we define damage $D^*$ as the life fraction $D^* = n/N_f$, where $n$ is

the number of cycles at a given stress and $N_f$ is the fatigue life, the number of cycles a volume of bone can resist prior to failure. Thus, the rate of damage accumulation is

$$\frac{dD^*}{dt} = D'_f - D'_r, \tag{7}$$

where $D'_f$ [day$^{-1}$] is the rate of damage accumulation and $D'_r$ [day$^{-1}$] is the rate of damage repair (Figure 2; pink box).

#### 2.3.1 Damage formation

Damage is incurred with each loading cycle (stride) and accumulates at faster rates at greater loads. The rate of damage accumulation $D'_f$ can therefore be expressed using the equation

$$D'_f = v_D(\sigma)v_n(t) = \frac{\partial D^*}{\partial n}\frac{dn}{dt}, \tag{8}$$

where $v_D(\sigma) = \partial D^*/\partial n$ is the damage accumulated per cycle and $v_n(t) = dn/dt$ is the number of cycles per day [12].

The ability of bone to resist fatigue at a particular stress level is characterised by the fatigue life $N_f$. Higher stresses impart greater damage to the bone, hypothesised to be due to the increased dissipation of mechanical energy into the bone [43]. Mechanical testing on equine subchondral bone has previously shown that the fatigue life of bone is related to the compressive stress (i.e. positive $\sigma$ corresponds to compression) of cycling through a power law:

$$N_f(\sigma) = 10^{-\frac{\sigma-\sigma_0}{\sigma_1}}, \tag{9}$$

where $\sigma_0 = 134.2$ MPa and $\sigma_1 = 14.1$ MPa [20]. Bone stiffness provides resistance to bone fatigue, thus, we adjust the fatigue life to include an additional multiplicative factor dependent on the Young's modulus [15, 39]:

$$N_f^*(\sigma) = N_f(\sigma)\frac{E}{E_{\text{nom}}} = 10^{-\frac{\sigma-\sigma_0}{\sigma_1}}\frac{E}{E_{\text{nom}}}, \tag{10}$$

where $E_{\text{nom}}$ is a reference stiffness. Given that Eq. (9) was derived from racehorses in training, we assume that $E_{\text{nom}} = E_0 \cdot 0.9^3 \cdot 0.36^{0.06} = 1714.1$ MPa, i.e. the experiments were conducted on bone with $f_{BM} = 0.9$ and a strain rate of 0.36 s$^{-1}$.

Since the bone fails at $D^* = 1$, the damage accumulated per cycle is

$$v_D(\sigma) = \frac{1}{N_f^*(\sigma)} = 10^{\frac{\sigma-\sigma_0}{\sigma_1}}\frac{E_{\text{nom}}}{E}. \tag{11}$$

While bone stiffness transiently increases before gradually decreasing over its fatigue lifetime [20], we have not included this phenomenon in the model for simplicity.

#### 2.3.2 Damage repair

Following the incursion of microdamage to bone, microcracks are removed by the resorption of bone by osteoclasts and subsequent bone formation (Figure 2; pink box). Bone remodelling occurs within bone multicellular units (BMUs) that contain populations of both osteoblasts and osteoclasts. Though microdamage is more likely to occur focally at loading sites [44], we model

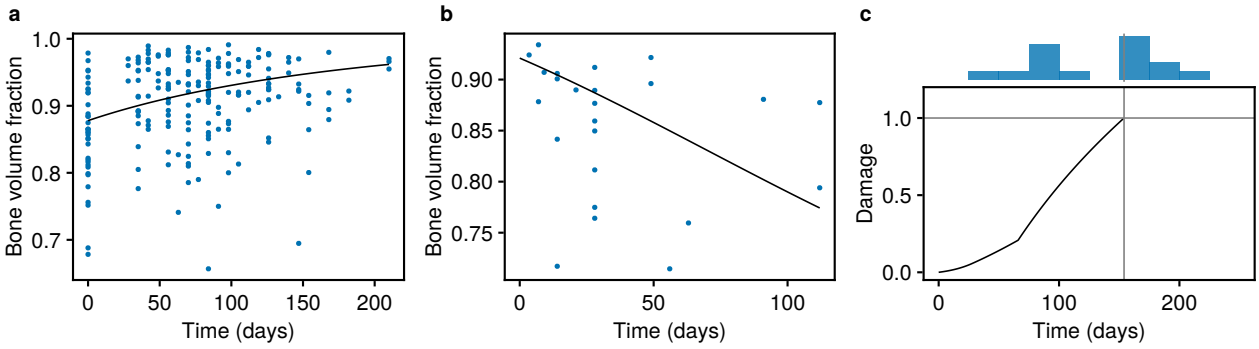


**Figure 3:** Comparisons of model output to bone volume fraction and time to fracture data [18]. The mathematical model has been fit to data (details in Subsection A.3, electronic supplementary material), with parameter values in Table 1. (a) Adaptation of bone volume fraction ($f_{BM}$) in response to training; (b) De-adaptation of bone volume fraction to rest. For (a) and (b), black lines indicate model simulations, and blue dots indicate data points. (c) Simulation of a fracture at high workloads, where the fracture occurs when the damage $D^*$ reaches 1, at which point the simulation is terminated. A histogram of the duration of preparations prior to fracture is shown above the main plot, with the median indicated with a vertical grey line.

microdamage as an even distribution throughout the entire volume of subchondral bone. Thus, the damage repair term in Eq. (7) is

$$D_r' = [A_{\text{OBL}} + (F_s - 1)A_{\text{OCL}}]\frac{\alpha S_v D^*}{f_{BM}}, \tag{12}$$

with a full derivation provided in Subsection A.1 of the electronic supplementary material. Briefly, bone formation ($A_{\text{OBL}}$) leads to a reduction of damage due to the dilution of microcracks across a larger volume. Bone resorption also leads to damage repair if osteoclasts target microcracks specifically. It has been observed that bone resorption is more likely to occur at sites of microcracks [45, 46]. Accordingly, we include a damage repair specificity factor, $F_s$ [dimensionless], which is the rate at which bone resorption sites co-localise with microcracks relative to the random emergence of resorption sites [15]. Thus, $F_s = 1$ corresponds to untargeted resorption. Following Martin [15], we set $F_s = 5$, since cracks are estimated to be 4–6 times more likely to be associated with resorption sites compared to chance alone [45, 46].

# 3 Results

## 3.1 Comparison of mathematical model to data

The model is calibrated to cross-sectional data on bone volume fraction and the median time in training for horses that sustained fractures [18, 24, 47, 48] (details in Subsection A.3, electronic supplementary material). Parameter estimation is performed using optimisation [49, 50], and comparisons of model simulations to data are shown in Figure 3. The response of bone to training and rest are depicted in Figures 3a and 3b respectively. Despite the marked variance within the data, the model captures trends including the gradual increase in bone volume fraction with training and more rapid loss of bone in response to rest. Furthermore, the model faithfully fits the median time to fracture (154 days) under a high workload (Figure 3c).

The parameters used in the model (including fitted parameters) are given in Table 1. Fits of the model to subsets of the data, grouped by horse age, sex and left/right limb, are shown in Figures S9–S11 of the electronic supplementary material.

**Table 1:** Parameters in the mathematical model of subchondral bone adaptation in Thoroughbred racehorses, and their ranges for sensitivity analysis.

| Parameter | Description | Units | Value [Initial (fitted)] | Range | Reference |
|---|---|---|---|---|---|
| $\sigma$ | Joint contact pressure | MPa | 81.1 | $[30.0, 102.0]$ | [a] |
| $\dot{\varepsilon}$ | Strain rate | $s^{-1}$ | 0.2974 | $[0.05, 0.46]$ | [a] |
| $v_n$ | Number of cycles per day | $day^{-1}$ | 43.7 | $[25.0, 120.0]$ | [a] |
| $\alpha$ | Fraction of specific surface | – | 0.19 | $[0.095, 0.285]$ | Whitton et al. [44] |
| $a$ | Fitting parameter relating $f_{BM}$ to $S_v$ | $mm^{-1}$ | 11.42 | $[5.71, 17.13]$ | Hitchens et al. [18] |
| $b$ | Fitting parameter relating $f_{BM}$ to $S_v$ | – | $-0.02$ | $[-0.2, 0.2]$ | Hitchens et al. [18] |
| $E_0$ | Maximum bone stiffness | MPa | 2500 | $[1250.0, 3750.0]$ | Martig et al. [20] |
| $\gamma_E$ | Exponent of strain rate in stiffness equation | – | 0.06 | $[0.03, 0.09]$ | Carter and Hayes [51] |
| $A_{\mathrm{OBL}}^{\min}$ | Minimum bone formation rate | mm/day | 0.001094 | $[0.0, 0.00301]$ | Firth et al. [22] |
| $A_{\mathrm{OBL}}^{\max}$ | Maximum bone formation rate | mm/day | 0.0127 (0.00603) | $[0.00301, 0.00904]$ | Davies [21] |
| $\delta_B$ | Half-saturation stress of bone formation | MPa | 7 | $[3.5, 10.5]$ | Les et al. [52] |
| $\gamma_B$ | Sigmoidicity of bone formation | – | 1 | $[1.0, 5.0]$ | Hitchens et al. [18] |
| $A_{\mathrm{OCL}}^{\min}$ | Minimum bone resorption rate | mm/day | 0.001 | $[0.0, 0.0018]$ | Boyde and Firth [33] |
| $A_{\mathrm{OCL}}^{\max}$ | Maximum bone resorption rate | mm/day | 0.011 (0.00358) | $[0.0018, 0.0054]$ | Boyde and Firth [33] |
| $\delta_C$ | Half-saturation stress of bone resorption | MPa | 1 | $[0.5, 1.5]$ | [b] |
| $\gamma_C$ | Sigmoidicity of bone resorption | – | 2 | $[1.0, 5.0]$ | [b] |
| $\sigma_0$ | Fitting parameter relating stress to fatigue life | MPa | 134.2 (139.5) | $[125.5, 153.4]$ | Martig et al. [20] |
| $\sigma_1$ | Fitting parameter relating stress to fatigue life | MPa | 14.1 | $[12.69, 15.51]$ | Martig et al. [20] |
| $E_{\mathrm{nom}}$ | Reference stiffness for stress-fatigue life equation | MPa | 1714.1 | $[857.0, 2571.2]$ | [c] |
| $F_s$ | Damage repair specificity factor | – | 5 | $[1.0, 10.0]$ | Martin [15] |

[a] Calculated from equations in Subsection A.2 of the electronic supplementary material with a speed of 14.0 m/s and a distance of 8000m every 30 days (Table 2, programme group 2 of Morrice-West et al. [27]). [b] Selected to achieve four times higher resorption in full training relative to rest [24]. [c] Calculated assuming $f_{BM} = 0.9$.

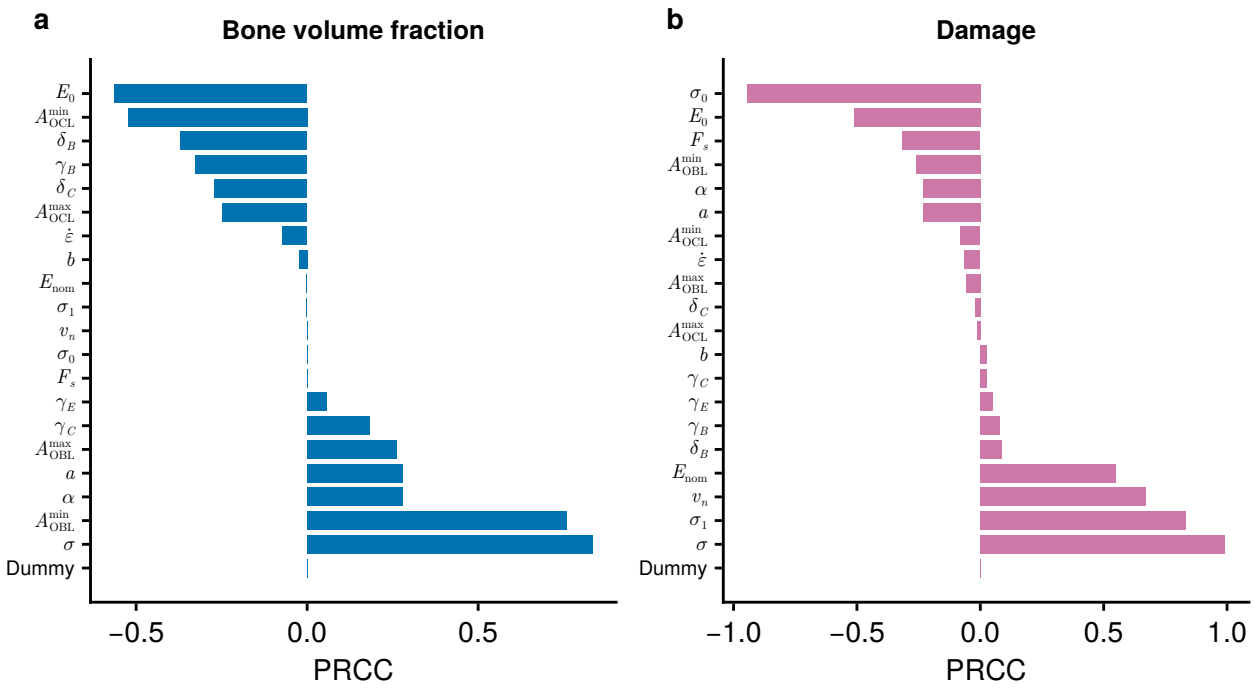


**Figure 4:** Sensitivity analysis of parameters using the partial rank correlation coefficient (PRCC). Effects of each parameter on (a) bone volume fraction $f_{BM}$; and (b) damage $D^*$ after 10 weeks. PRCC values of high magnitude indicate parameters with a consistent influence on the output variables of interest, with the sign indicating the direction of correlation. The model described by Eqs (1)–(12) is simulated using an initial condition of $f_{BM} = 0.7$ and $D^* = 0$. Descriptions of parameters and their ranges are shown in Table 1. A dummy variable with no effect on the output has been included to detect potentially spurious relationships.

## 3.2 Sensitivity of bone volume fraction and damage to parameters

Initial simulations of the calibrated model under varying stresses $\sigma$ indicate that both bone volume fraction and damage accumulation increase in response to higher joint stresses (Subsection B.1, electronic supplementary material). To generalise this analysis to all model parameters, we use a sensitivity analysis (details in Subsection A.4, electronic supplementary material) to identify the parameters that produce the greatest changes in bone volume fraction and damage. Figure 4 shows the results from this sensitivity analysis, using the partial rank correlation coefficient (PRCC) as the sensitivity measure [53]. Under this measure, parameters with very positive (negative) sensitivities tend to increase (decrease) the output variable most consistently. The parameters $\sigma$, $A_{\mathrm{OBL}}^{\mathrm{min}}$ and $A_{\mathrm{OBL}}^{\mathrm{max}}$ are among those that increase $f_{BM}$ the most consistently (Figure 4a). This is expected, due to the role of stress and osteoblast activity in bone formation. The surface area parameters $a$ and $\alpha$ also have a tendency to increase bone volume fraction, although this may be because our simulations are more likely to correspond to bone formation than resorption. The bone stiffness $E_0$ is the parameter most consistently associated with loss of bone, followed by $A_{\mathrm{OCL}}^{\mathrm{min}}$, $\delta_B$ and $\gamma_B$. The bone stiffness $E_0$ has a negative PRCC because it inhibits the mechanical signal required for bone formation (Eq. (3)). Unsurprisingly, increasing the rate of bone resorption through $A_{\mathrm{OCL}}^{\mathrm{min}}$ leads to a loss of bone mass. The parameters $\delta_B$ and $\gamma_B$ appear to reduce the bone formation rates at low strain energy densities, and as a result lead to a net loss of bone mass.

The stress $\sigma$ and cycles per day $v_n$ are among the most consistent inducers of bone damage $D^*$ (Figure 4b). Other parameters that tend to increase bone damage are $\sigma_1$ and $E_{\mathrm{nom}}$. The

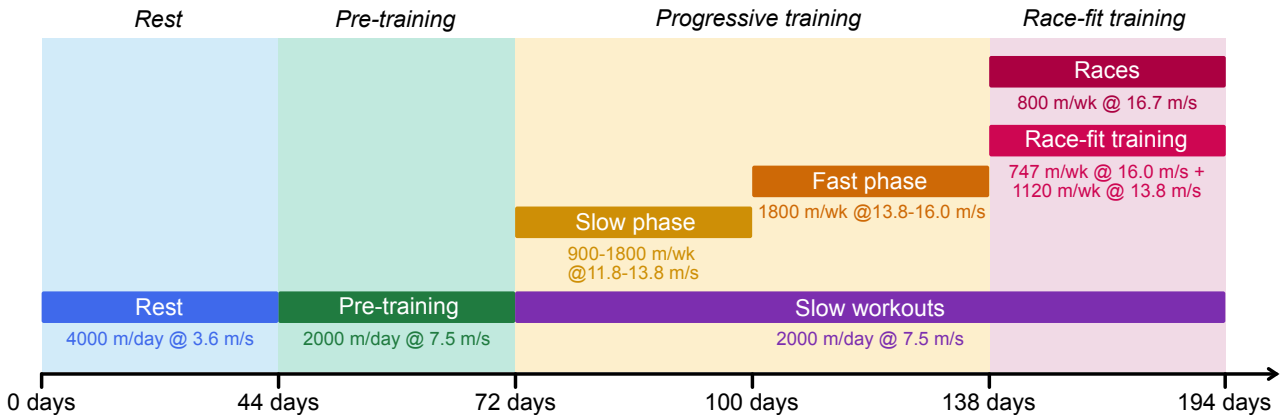


**Figure 5:** Schematic of the simulated training program (*'preparation'*). Note that time starts from the start of a rest period and is not shown to scale. Distances for longer-distance training at canter speeds and below are expressed in distances per day, whereas faster workouts (which are not performed every day) are expressed in distances per week.

parameter most associated with reduced damage is $\sigma_0$, due to its ability to offset stresses in the exponential relationship between stress and fatigue life (Eq. (9)). $E_0$ and $F_s$ are also able to reduce bone damage, indicating the role that bone stiffness and microdamage resorption play in resisting failure.

While the PRCC reliably estimates the manner in which a parameter affects an output, it may fail to capture the relative magnitude of these effects [54]. The Sobol index is an alternative parameter sensitivity measure that accounts for the magnitude of changes [55, 56]. In line with the PRCC, results for Sobol indices show that the stress is a major factor contributing to bone volume fraction and damage, and that cycles per day has a strong influence on damage (Subsection B.2, electronic supplementary material). The sensitivities for most parameters are largely independent of time (Figures S12–S13, electronic supplementary material).

### 3.3 Temporal response of bone to training programs

The sensitivity analysis only considers training programs that are constant in time. To account for changes in training regimes as racehorses progress from rest to racing, we model the response of bone to a typical Australian training and racing preparation [27, 57–60], as summarised in Figure 5 (details in Subsection A.2, electronic supplementary material). We assume horses start training in their 2-year-old season (in the southern hemisphere, after 1 August in the year that they turn 2-years-old) with an initial bone volume fraction of $f_{BM} = 0.61$ and zero damage. While two-year-old horses are trained at smaller distances compared to mature horses [27], we have assumed for simplicity that training programs are constant over a horse's career. The bone is simulated over four preparations consisting of rest, pre-training, progressive training and race-fit training, and results are shown in Figure 6. The bone volume fraction gradually increases from preparation to preparation, but varies between 0.86 and 0.93 during the fourth preparation, consistent with values seen in horses at rest and training respectively [20]. The damage corresponding to this training program rises during both progressive training and race-fit training, to a value of $D^* = 0.73$ by the end of the first racing preparation. The damage is repaired during the subsequent rest period, although the repair processes are unable to completely remove this damage. While progressive training resumes before the damage has completely repaired, the maximum damage attained in subsequent preparations is approximately equal to that at the end of the first preparation.

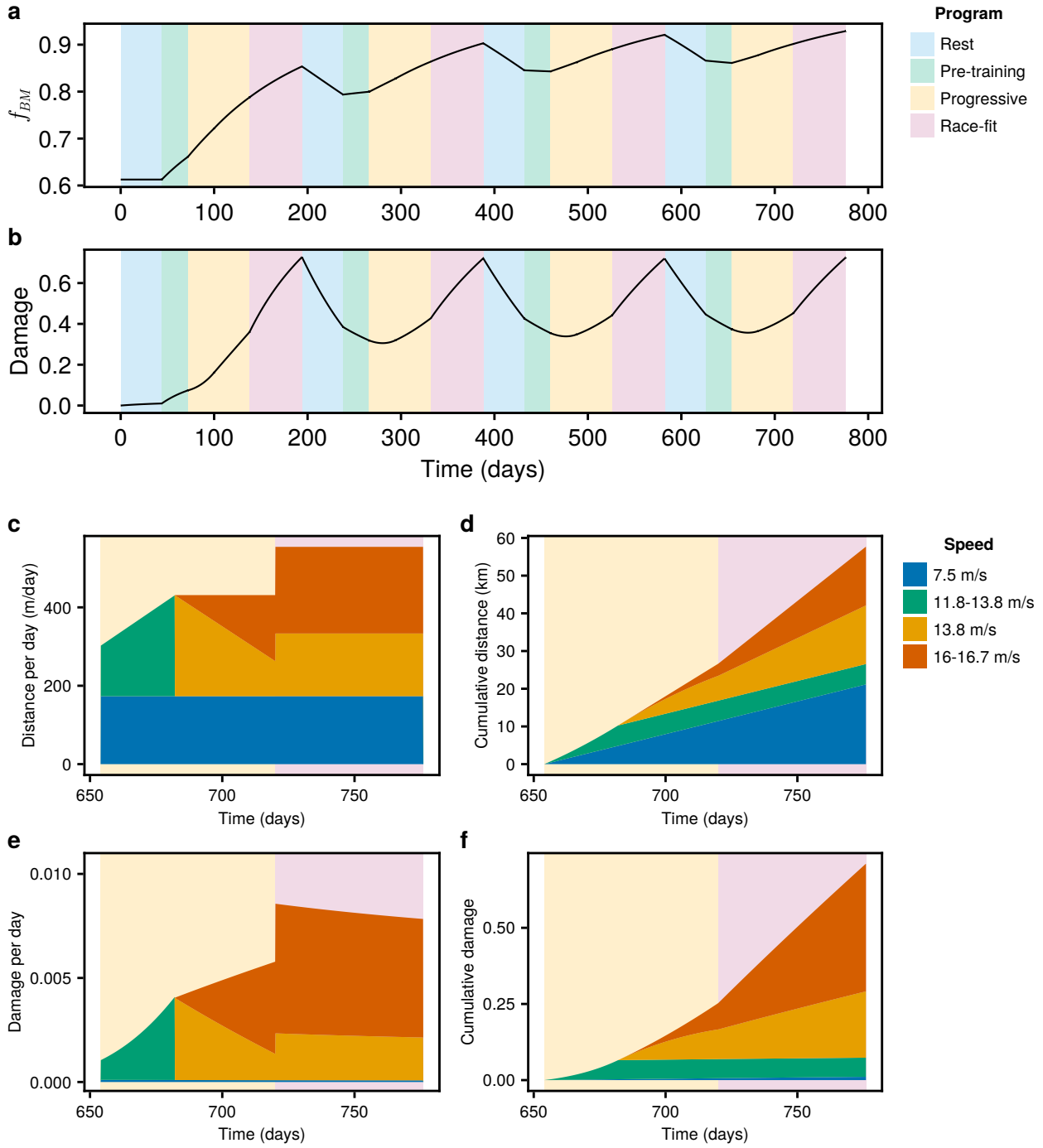


**Figure 6:** Dynamic simulations of bone in response to training program. The training program is described in Subsection A.2 of the electronic supplementary material, with backgrounds used to indicate periods of rest (blue), pre-training (green), progressive training (yellow) and race-fit training (pink). Simulations are run starting from $f_{BM} = 0.61$ and $D^* = 0$, corresponding to an untrained racehorse. The simulation is run over four preparations. Changes in (a) bone volume fraction $f_{BM}$ and (b) damage $D^*$ are plotted against time. During the final (fourth) instance of progressive and race-fit training ($t \in [654, 776]$), the distance and damage accumulated at speeds $\geq 7.5$ m/s are summarised in (c–f). (c) Distance per day; (d) cumulative distance; (e) damage per day; and (f) cumulative damage.

A breakdown of the distances accumulated during the final (fourth) progressive and race-fit training preparations is plotted in Figure 6c. The distances are coloured according to the corresponding speeds. There is a gradual increase in distances covered at the highest speed of 16.0 m/s as the horse shifts from progressive training (yellow background) to racing (pink background). By the end of the racing period, the horse has covered 57.7 km, with 21.1 km at canter (7.5 m/s), 15.6km at racing speed (16.0–16.7 m/s), 15.5 km at a fast gallop (13.8 m/s) and 5.4 km at slow gallop (11.8–13.8 m/s) (Figure 6d). The damage accumulated per day is plotted in Figure 6e, and the resulting cumulative damage is shown in Figure 6f. High speeds above 13.8 m/s account for the majority of damage accumulated during training (Figure 6f).

## 4 Discussion

In this study, we present a new mathematical model coupling the dynamics of bone adaptation and bone damage in the subchondral bone of the distal third metacarpus of Thoroughbred racehorses. Our model expands on a previous model of bone adaptation [18] through the addition of a dynamic resorption rate and variables accounting for bone damage. The coupling of bone adaptation and damage dynamics enables new analyses of the response of bone to training. This includes a sensitivity analysis of the parameters most relevant for bone damage, and estimates of how bone damage dynamically evolves in response to various phases of training.

Our model is consistent with data relating to both bone volume fraction and median times to fracture during a racing preparation (Figure 3). Our previous model was already consistent with bone volume fraction [18], and our fits in this current work confirm that bone resorption at rest occurs at faster rates than bone formation in training ($f_{BM}$ increases by 0.053 in response to 100 days of training in Figure 3a, but decreases by 0.131 in response to 100 days of rest in Figure 3b). However, the two models differ in the time taken for a steady state to be achieved during rest (Figure 3b). Further investigation is required to better characterise de-adaptation times in racehorses. In addition to fitting changes in bone volume fraction, we fit our model to data on horses that had sustained a fracture [18], observing a time to failure consistent with their time in training. However, we note that this fit requires revising our estimate of $\sigma_0$ from 134.2 MPa to 139.5 MPa (Table 1). From Eq. (11), this corresponds to an estimated 57.8% reduction in damage formation rate compared to the relationship derived by Martig et al. [20]. We speculate that this discrepancy is due to differences in forces that bones experience *in vitro* compared to *in vivo*. Martig et al. [20] performed unconfined mechanical tests on subchondral bone cylinders extracted from the lateral condyle of the third metacarpal bone. However, bone in reality is surrounded by bone and overlying cartilage *in vivo* [61]. Thus, we expect that these surrounding structures would absorb some of the applied stress, mitigating the extent of damage incurred on the subchondral bone sample being modelled. The application of finite-element models of the metacarpophalangeal joint may provide a means for accounting for these effects [62], but has yet to be applied to galloping horses.

Our sensitivity analysis identifies key parameters affecting bone volume fraction and induction of bone damage. We find that the stress $\sigma$ is a major factor contributing to both bone formation and damage, having positive PRCC values (Figure 4) and being the highest ranked parameter on the Sobol index (Figure S7, electronic supplementary material). These results are consistent with previous studies on racehorses, which find that (i) training is associated with higher bone volume fractions in racehorses [24, 33]; (ii) high acute workloads are associated with higher rates of musculoskeletal injuries [6]; and (iii) bone failure is accelerated by the application of stresses of higher magnitude [20]. While the number of cycles per day $v_n$ has virtually no influence on bone volume fraction (Figure 4a), it is a strong inducer of bone damage, according to both

the PRCC and Sobol index (Figures 4b,S7b, electronic supplementary material). This finding lends support to previous studies that have observed increased rates of musculoskeletal injury in horses that accumulate greater distances during training [6, 7].

The sensitivity of bone damage to both stress and cycles per day are subject to strong interactions between parameters (Figure S7b, electronic supplementary material). In particular, among pairs of parameters involving the cycles per day $v_n$, the pair ($\sigma$,$v_n$) has the highest second-order Sobol index (Figure S7c, electronic supplementary material). Since both high stress and high cycles per day are required for the formation of damage, it is conceivable that the effects on bone damage could be mitigated by restricting distances accrued at higher speeds. Thus, though we may speculate that 'fast and light' training programs [27] are less likely to result in injuries than higher volume programs, they were only associated with fewer injuries in two-year-old racehorses, and not mature racehorses [7]. A possible explanation for the lack of significant association in mature racehorses is the role of pre-existing injury and damage in causing future injuries, and that low grade injury is more tolerated in older racehorses.

The sensitivity values (using either PRCC or Sobol indices) can have a range of interpretations, depending on the nature of each parameter. Parameters such as $v_n$, $\sigma$ and $\dot{\varepsilon}$ are external to the system and controllable through the design of training programs [53]. In this context, sensitivities characterise the effect of varying these parameters on our outputs of interest, namely the bone volume fraction $f_{BM}$ and damage $D^*$. The other parameters are internal to the bone remodelling system and are often difficult or impossible to influence. Variations in these parameters may represent either uncertainties in the measurements of these parameters or biological heterogeneities inherent within the population. High sensitivities for these parameters point towards sources of uncertainty or variation in our estimates of model outputs [63]. We expect that gaining better confidence in these sensitive parameters (on either a population or individual level) through future studies would help us to model bone adaptation and damage more accurately. On the other hand, variation or uncertainty in insensitive parameters are less likely to be important in estimating $f_{BM}$ and $D^*$, although we note that they may have consequential effects on other variables of interest. In our model, we find that the parameter $\sigma_0$ has a large effect in simulating damage (Figure S7b, electronic supplementary material). While this parameter is fitted to observational data by comparing to a median time to fracture, substantial variation exists between racehorses (Figure 3c,f) and between age groups (Figure S9c, electronic supplementary material). Thus, while microdamage is difficult to quantify in living racehorses (i.e. prior to catastrophic fracture), we believe that further work on understanding microdamage accumulation *in vivo* is warranted. We also find relatively high Sobol sensitivities in bone volume fraction to $A^{\min}_{\mathrm{OBL}}$, $A^{\min}_{\mathrm{OCL}}$ and $E_0$ (Figure S7a, electronic supplementary material). Thus, better estimates of bone formation and resorption rates would aid in the simulation of bone volume fraction. While bone stiffness $E_0$ has been measured in racehorses, it greatly varies between horses [20], and incorporating the effects of this heterogeneity would be of interest for future work.

We use our model to simulate the response of bone volume fraction and damage in response to a dynamic training program including rest, progressive training and race-fit training (Figure 6). We find that fluctuations in bone volume fraction (Figure 6a) are consistent with those observed in horses resting and in training [24]. While bone microdamage is more difficult to measure, our model suggests that both progressive and race-fit training contribute to damage, with higher speed ($\geq$ 13.8 m/s) training accounting for the majority of damage (Figure 6f). Our model indicates that distances accumulated at canter speeds do not contribute substantially to damage (Figure 6f). However, prior studies have linked high canter distances to musculoskeletal injury

when combined with high gallop distances [6]. This warrants further investigation, although we note that Verheyen et al. [6] categorise relatively fast speeds of up to 14 m/s as canter.

Our model simulations indicate that during training, bone damage does not plateau in time, and therefore all bones will eventually fail unless given the opportunity to repair damage through rest (Figure 6b). Holmes et al. [24] found lower rates of bone remodelling in training racehorses relative to resting racehorses, and on this basis recommend frequent rest to allow the bone to repair. While bone remodelling can occur during training, our model suggests that the repair associated with remodelling is insufficient to prevent the eventual failure of bone in response to prolonged training. In Victoria, Australia, rest periods can vary between 2–16 weeks, with the average reported to be 6.3 weeks in mature racehorses [7, 27]. Our model suggests that bone damage does not fully repair over a rest period of 6.3 weeks (Figure 6b), and therefore longer (or more frequent) rest periods are likely to benefit the repair of damage.

While previous models have coupled bone remodelling and damage [12, 13, 15, 38], we believe our study is the first to model these two processes dynamically in racehorses. Our model is calibrated to data on bone volume fractions and time to fracture from racehorses in training and rest. In contrast to the aforementioned studies [12, 15, 38], we do not observe reduced bone volume fraction in response to intense loading. This discrepancy is possibly because previous models account for the induction of bone remodelling in response to damage. We have not incorporated this process in our model as third metacarpal bone volume fractions tend to increase near failure [64], possibly due to the inhibition of bone resorption at high loads [24]. However, focal bone resorption sites appear in response to damage, and are associated with fracture [44]. Further work is required to investigate the role of focal remodelling in bone injury. In the context of racehorses, Shaffer et al. [65] use a compartmental model to account for transitions between undamaged, damaged and resorbed bone. However, this model is analysed under the assumption of steady state and does not directly model the effects of exercise on transition rates. In contrast to our model, Shaffer et al. [65] find increased resorption rates associated with training in damaged regions of bone, possibly due to the appearance of focal remodelling at sites of fracture [44].

Given the cross-sectional nature of our data, there is substantial variation in the data used to fit our model (Figure 3), which we acknowledge as a limitation. The population of horses within the dataset exhibit variation in several characteristics known to be associated with catastrophic musculoskeletal injury [8] – such as age, sex, training practices and racing surfaces – that may also affect the dynamics of bone adaptation and microdamage [7, 66–68]. Although it would be valuable to examine how heterogeneities within the racehorse population might affect our findings, we do not believe the data used is sufficient to allow for such an analysis. We provide fits of our model to subsets of the data, grouped by age, sex, and left/right limb (Figures S9–S11, electronic supplementary material), but further work is needed to reliably infer relationships between horse demographics and biological parameters. Additionally, parameters such as osteoblast and osteoclast activity, as well as training speed and distance, are known to vary with age [27, 69]. For the purposes of this study, we have assumed these parameters to be constant in time (Figure 6). However, future work could incorporate age-varying training programs using training information reported by racehorse trainers [27].

As with our previous work [18], this study is limited by the use of a lumped parameter model. While we employ a lumped parameter model for computational efficiency, bone stresses, microdamage and repair processes are not evenly distributed throughout the bone [70–72]. Bergstrom et al. [73] have found associations between parasagittal groove fractures with more frequent rest and increased loads prior to bone injury. It would be of interest to incorporate

our bone adaptation and damage equations into a finite-element model of bone mechanics to investigate these spatial heterogeneities [35, 62]. We also recognise that biochemical signalling and evolution of osteoblast and osteoclast densities may play a role in bone dynamics, causing delays in the response of bone to exercise [74, 75] and also providing the tissue with memory of the stresses incurred during the preceding days [76–78]. Accounting for these processes will enable better quantification of the response of bone to training programs that rapidly alternate between intense and less intense exercise. For simplicity, we have made the assumption that bone stiffness is independent of damage. While the stiffness of subchondral bone is well maintained for the majority of its fatigue life [20], this loss of stiffness could lead to feedback on the dynamics of bone remodelling. The number of cycles per day can influence bone adaptation [79]. However, we have not modelled this relationship as bone formation has been observed to plateau above 36 cycles per day [79], and we assume that horses train at distances above this threshold. Finally, substantial variability exists on the level of both horses and trainers [27]. More detailed training and bone material property data is required to quantify heterogeneity in the bone adaptation parameters across populations of racehorses and to understand the effect of different training programs on bone injury.

# 5 Conclusion

We have developed a new mathematical model that couples the processes of bone adaptation and damage in the metacarpal subchondral bone of Thoroughbred racehorses. Our model is consistent with measurements of bone volume fraction and damage in response to rest and training. Simulations of the model indicate that applied stresses and the number of cycles per day are among the most important parameters in determining bone damage. Over the course of a typical racing preparation in Victoria, Australia, our model estimates that cycles accumulated at racing speeds are responsible for the majority of the damage. Our findings suggest that extended or more frequent rest periods are likely to be beneficial in repairing bone damage with the aim of preventing fractures in racehorses.

## 5.1 Funding

This study was funded by the Hong Kong Jockey Club Equine Welfare Research Foundation and was in part conducted under the Equine Limb Injury Prevention Research Program funded by Racing Victoria Ltd. (RVL), the Victorian Racing Industry Fund (VRIF) of the Victorian State Government, and the University of Melbourne.

## 5.2 Conflict of Interest

The authors declare no conflicts of interest.

## 5.3 Data availability

The code associated with this manuscript is available from https://github.com/mic-pan/equine_bone_fatigue. Since the data is owned by proprietary bodies and not available for distribution, the code for model calibration has been redacted.

## References


1. Johnson BJ, *et al.*, 1994. Causes of death in racehorses over a 2 year period. *Equine Veterinary Journal* **26**(4), 327–330. doi:10.1111/j.2042-3306.1994.tb04395.x

2. Stover SM, 2017. Nomenclature, classification, and documentation of catastrophic fractures and associated preexisting injuries in racehorses. *Journal of Veterinary Diagnostic Investigation* **29**(4), 396–404. doi:10.1177/1040638717692846

3. Gibson MJ, Legg KA, Gee EK, Rogers CW, 2023. The reporting of racehorse fatalities in New Zealand Thoroughbred flat racing in the 2011/12–2021/22 seasons. *Animals* **13**(4), 612. doi:10.3390/ani13040612

4. Kawcak CE, McIlwraith CW, Norrdin RW, Park RD, Steyn PS, 2000. Clinical effects of exercise on subchondral bone of carpal and metacarpophalangeal joints in horses. *Am. J. Vet. Res.* **61**(10), 1252–1258. doi:10.2460/ajvr.2000.61.1252

5. Martig S, Chen W, Lee PVS, Whitton RC, 2014. Bone fatigue and its implications for injuries in racehorses. *Equine Vet. J.* **46**(4), 408–415. doi:10.1111/evj.12241

6. Verheyen K, Price J, Lanyon L, Wood J, 2006. Exercise distance and speed affect the risk of fracture in racehorses. *Bone* **39**(6), 1322–1330. doi:10.1016/j.bone.2006.05.025

7. Wong ASM, Morrice-West AV, Hitchens PL, Whitton RC, 2023. The association between Thoroughbred racehorse training practices and musculoskeletal injuries in Victoria, Australia. *Frontiers in Veterinary Science* **10**, 1260554. doi:10.3389/fvets.2023.1260554

8. Hitchens PL, Morrice-West AV, Stevenson MA, Whitton RC, 2019. Meta-analysis of risk factors for racehorse catastrophic musculoskeletal injury in flat racing. *Veterinary Journal* **245**, 29–40. doi:10.1016/j.tvjl.2018.11.014

9. Meslier QA, Shefelbine SJ, 2023. Using finite element modeling in bone mechanoadaptation. *Current Osteoporosis Reports* **21**(2), 105–116. doi:10.1007/s11914-023-00776-9

10. Pivonka P, Calvo-Gallego JL, Schmidt S, Martínez-Reina J, 2024. Advances in mechanobiological pharmacokinetic-pharmacodynamic models of osteoporosis treatment – pathways to optimise and exploit existing therapies. *Bone* **186**, 117140. doi:10.1016/j.bone.2024.117140

11. Hazelwood SJ, Castillo AB, 2007. Simulated effects of marathon training on bone density, remodeling, and microdamage accumulation of the femur. *International Journal of Fatigue* **29**(6), 1057–1064. doi:10.1016/j.ijfatigue.2006.10.001

12. van Oers RFM, van Rietbergen B, Ito K, Huiskes R, Hilbers PAJ, 2011. Simulations of trabecular remodeling and fatigue: Is remodeling helpful or harmful? *Bone* **48**(5), 1210–1215. doi:10.1016/j.bone.2011.01.011

13. Martínez-Reina J, Calvo-Gallego JL, Pivonka P, 2021. Combined effects of exercise and denosumab treatment on local failure in post-menopausal osteoporosis–insights from bone remodelling simulations accounting for mineralisation and damage. *Frontiers in Bioengineering and Biotechnology* **9**, 635056. doi:10.3389/fbioe.2021.635056

14. Martínez-Reina J, Calvo-Gallego JL, Martin M, Pivonka P, 2022. Assessment of strategies for safe drug discontinuation and transition of denosumab treatment in PMO—insights from a mechanistic PK/PD model of bone turnover. *Frontiers in Bioengineering and Biotechnology* **10**, 886579. doi:10.3389/fbioe.2022.886579

15. Martin B, 1995. Mathematical model for repair of fatigue damage and stress fracture in osteonal bone. *J. Orthop. Res.* **13**(3), 309–316. doi:10.1002/jor.1100130303

16. Taylor D, Casolari E, Bignardi C, 2004. Predicting stress fractures using a probabilistic model of damage, repair and adaptation. *J. Orthop. Res.* **22**(3), 487–494. doi:10.1016/j.orthres.2003.08.022

17. Buenzli PR, Jeon J, Pivonka P, Smith DW, Cummings PT, 2012. Investigation of bone resorption within a cortical basic multicellular unit using a lattice-based computational model. *Bone* **50**(1), 378–389. doi:10.1016/j.bone.2011.10.021

18. Hitchens PL, Pivonka P, Malekipour F, Whitton RC, 2018. Mathematical modelling of bone adaptation of the metacarpal subchondral bone in racehorses. *Biomech. Model. Mechanobiol.* **17**(3), 877–890. doi:10.1007/s10237-017-0998-z

19. Morrice-West AV, *et al.*, 2022. Relationship between Thoroughbred workloads in racing and the fatigue life of equine subchondral bone. *Sci. Rep.* **12**(11528), 1–11. doi:10.1038/s41598-022-14274-y

20. Martig S, Lee PVS, Anderson GA, Whitton RC, 2013. Compressive fatigue life of subchondral bone of the metacarpal condyle in thoroughbred racehorses. *Bone* **57**(2), 392–398. doi:10.1016/j.bone.2013.09.006

21. Davies HMS, 1995. *The adaptive response of the equine metacarpus to locomotory stress.* PhD thesis, University of Melbourne, Australia

22. Firth EC, Rogers CW, Doube M, Jopson NB, 2005. Musculoskeletal responses of 2-year-old Thoroughbred horses to early training. 6. Bone parameters in the third metacarpal and third metatarsal bones. *N. Z. Vet. J.*

23. Wang X, *et al.*, 2016. A mechanostatistical approach to cortical bone remodelling: an equine model. *Biomech. Model. Mechanobiol.* **15**(1), 29–42. doi:10.1007/s10237-015-0669-x

24. Holmes JM, Mirams M, Mackie EJ, Whitton RC, 2014. Thoroughbred horses in race training have lower levels of subchondral bone remodelling in highly loaded regions of the distal metacarpus compared to horses resting from training. *Vet. J.* **202**(3), 443–447. doi:10.1016/j.tvjl.2014.09.010

25. Murray RC, Vedi S, Birch HL, Lakhani KH, Goodship AE, 2001. Subchondral bone thickness, hardness and remodelling are influenced by short-term exercise in a site-specific manner. *J. Orthop. Res.* **19**(6), 1035–1042. doi:10.1016/S0736-0266(01)00027-4

26. Hazelwood SJ, Bruce Martin R, Rashid MM, Rodrigo JJ, 2001. A mechanistic model for internal bone remodeling exhibits different dynamic responses in disuse and overload. *Journal of Biomechanics* **34**(3), 299–308. doi:10.1016/S0021-9290(00)00221-9

27. Morrice-West AV, Hitchens PL, Walmsley EA, Stevenson MA, Whitton RC, 2020. Training practices, speed and distances undertaken by Thoroughbred racehorses in Victoria, Australia. *Equine Vet. J.* **52**(2), 273–280. doi:10.1111/evj.13156

28. Witte TH, Hirst CV, Wilson AM, 2006. Effect of speed on stride parameters in racehorses at gallop in field conditions. *J. Exp. Biol.* **209**(21), 4389–4397. doi:10.1242/jeb.02518

29. Lerebours C, Thomas CDL, Clement JG, Buenzli PR, Pivonka P, 2015. The relationship between porosity and specific surface in human cortical bone is subject specific. *Bone* **72**, 109–117. doi:10.1016/j.bone.2014.11.016

30. Colloca M, Blanchard R, Hellmich C, Ito K, van Rietbergen B, 2014. A multiscale analytical approach for bone remodeling simulations: Linking scales from collagen to trabeculae. *Bone* **64**, 303–313. doi:10.1016/j.bone.2014.03.050

31. You L, *et al.*, 2008. Osteocytes as mechanosensors in the inhibition of bone resorption due to mechanical loading. *Bone* **42**(1), 172–179. doi:10.1016/j.bone.2007.09.047

32. da Silva RGC, *et al.*, 2024. Intracortical remodelling increases in highly loaded bone after exercise cessation. *Journal of Anatomy* **244**(3), 424–437. doi:10.1111/joa.13969

33. Boyde A, Firth EC, 2005. Musculoskeletal responses of 2-year-old Thoroughbred horses to early training. 8. Quantitative back-scattered electron scanning electron microscopy and confocal fluorescence microscopy of the epiphysis of the third metacarpal bone. *N. Z. Vet. J.*

34. Seref-Ferlengez Z, Kennedy OD, Schaffler MB, 2015. Bone microdamage, remodeling and bone fragility: how much damage is too much damage? *BoneKEy Reports* **4**. doi:10.1038/bonekey.2015.11

35. Malekipour F, Whitton RC, Lee PVS, 2020. Distribution of mechanical strain in equine distal metacarpal subchondral bone: A microct-based finite element model. *Med. Novel Technol. Devices* **6**, 100036. doi:10.1016/j.medntd.2020.100036

36. Whitton RC, Ayodele BA, Hitchens PL, Mackie EJ, 2018. Subchondral bone microdamage accumulation in distal metacarpus of Thoroughbred racehorses. *Equine Veterinary Journal* **50**(6), 766–773. doi:10.1111/evj.12948

37. Carter DR, Caler WE, 1985. A cumulative damage model for bone fracture. *J. Orthop. Res.* **3**(1), 84–90. doi:10.1002/jor.1100030110

38. McNamara LM, Prendergast PJ, 2007. Bone remodelling algorithms incorporating both strain and microdamage stimuli. *J. Biomech.* **40**(6), 1381–1391. doi:10.1016/j.jbiomech.2006.05.007

39. García-Aznar JM, Rueberg T, Doblare M, 2005. A bone remodelling model coupling microdamage growth and repair by 3D BMU-activity. *Biomechanics and Modeling in Mechanobiology* **4**(2), 147–167. doi:10.1007/s10237-005-0067-x

40. Nyman JS, Yeh OC, Hazelwood SJ, Martin RB, 2004. A theoretical analysis of long-term bisphosphonate effects on trabecular bone volume and microdamage. *Bone* **35**(1), 296–305. doi:10.1016/j.bone.2004.03.007

41. McNamara BP, Taylor D, Prendergast PJ, 1997. Computer prediction of adaptive bone remodelling around noncemented femoral prostheses: the relationship between damage-based and strain-based algorithms. *Medical Engineering & Physics* **19**(5), 454–463. doi:10.1016/S1350-4533(97)00002-7

42. Pattin CA, Caler WE, Carter DR, 1996. Cyclic mechanical property degradation during fatigue loading of cortical bone. *Journal of Biomechanics* **29**(1), 69–79. doi:10.1016/0021-9290(94)00156-1

43. Shaktivesh S, Malekipour F, Whitton RC, Hitchens PL, Lee PVS, 2020. Fatigue behavior of subchondral bone under simulated physiological loads of equine athletic training. *J. Mech. Behav. Biomed. Mater.* **110**, 103920. doi:10.1016/j.jmbbm.2020.103920

44. Whitton RC, Mirams M, Mackie EJ, Anderson GA, Seeman E, 2013. Exercise-induced inhibition of remodelling is focally offset with fatigue fracture in racehorses. *Osteoporos. Int.* **24**(7), 2043–2048. doi:10.1007/s00198-013-2291-z

45. Burr DB, Martin RB, 1993. Calculating the probability that microcracks initiate resorption spaces. *J. Biomech.* **26**(4), 613–616. doi:10.1016/0021-9290(93)90023-8

46. Mori S, Burr DB, 1993. Increased intracortical remodeling following fatigue damage. *Bone* **14**(2), 103–109. doi:10.1016/8756-3282(93)90235-3

47. Williamson AJ, *et al.*, 2018. Biomechanical testing of the calcified metacarpal articular surface and its association with subchondral bone microstructure in Thoroughbred racehorses. *Equine Veterinary Journal* **50**(2), 255–260. doi:10.1111/evj.12748

48. Martig S, Hitchens PL, Lee PVS, Whitton RC, 2020. The relationship between microstructure, stiffness and compressive fatigue life of equine subchondral bone. *J. Mech. Behav. Biomed. Mater.* **101**, 103439. doi:10.1016/j.jmbbm.2019.103439

49. Storn R, Price K, 1997. Differential evolution – a simple and efficient heuristic for global optimization over continuous spaces. *J. Global Optim.* **11**(4), 341–359. doi:10.1023/A:1008202821328

50. Nocedal J, Wright SJ, 2006. *Numerical Optimization.* New York, NY, USA: Springer

51. Carter DR, Hayes WC, 1977. The compressive behavior of bone as a two-phase porous structure. *JBJS* **59**(7), 954

52. Les CM, Keyak JH, Stover SM, Taylor KT, Kaneps AJ, 1994. Estimation of material properties in the equine metacarpus with use of quantitative computed tomography. *J. Orthop. Res.* **12**(6), 822–833. doi:10.1002/jor.1100120610

53. Marino S, Hogue IB, Ray CJ, Kirschner DE, 2008. A methodology for performing global uncertainty and sensitivity analysis in systems biology. *J. Theor. Biol.* **254**(1), 178–196. doi:10.1016/j.jtbi.2008.04.011

54. Renardy M, Joslyn LR, Millar JA, Kirschner DE, 2021. To Sobol or not to Sobol? The effects of sampling schemes in systems biology applications. *Mathematical Biosciences* **337**, 108593. doi:10.1016/j.mbs.2021.108593

55. Sobol' IM, 2001. Global sensitivity indices for nonlinear mathematical models and their Monte Carlo estimates. *Math. Comput. Simul.* **55**(1), 271–280. doi:10.1016/S0378-4754(00)00270-6

56. Sobol' IM, Asotsky D, Kreinin A, Kucherenko S, 2011. Construction and Comparison of High-Dimensional Sobol' Generators. *Wilmott* **2011**(56), 64–79. doi:10.1002/wilm.10056

57. Whitton RC, *et al.*, 2019. Associations between pre-injury racing history and tibial and humeral fractures in Australian Thoroughbred racehorses. *Veterinary Journal* **247**, 44–49. doi:10.1016/j.tvjl.2019.03.001

58. Hampson BA, *et al.*, 2010. Monitoring distances travelled by horses using GPS tracking collars. *Australian Veterinary Journal* **88**(5), 176–181. doi:10.1111/j.1751-0813.2010.00564.x

59. Hodgson DR, 2014. Training the thoroughbred racehorse. In *The Athletic Horse (Second Edition)*, pp. 302–304. W.B. Saunders. doi:10.1016/B978-0-7216-0075-8.00029-0

60. Morrice-West AV, *et al.*, 2021. Variation in GPS and accelerometer recorded velocity and stride parameters of galloping Thoroughbred horses. *Equine Veterinary Journal* **53**(5), 1063–1074. doi:10.1111/evj.13370

61. Santschi EM, 2008. Articular fetlock injuries in exercising horses. *Vet. Clin. North Am. Equine Pract.* **24**(1), 117–132. doi:10.1016/j.cveq.2007.11.011

62. Harrison SM, Chris Whitton R, Kawcak CE, Stover SM, Pandy MG, 2014. Evaluation of a subject-specific finite-element model of the equine metacarpophalangeal joint under physiological load. *J. Biomech.* **47**(1), 65–73. doi:10.1016/j.jbiomech.2013.10.001

63. Gutenkunst RN, *et al.*, 2007. Universally sloppy parameter sensitivities in systems biology models. *PLOS Computational Biology* **3**(10), e189. doi:10.1371/journal.pcbi.0030189

64. Whitton RC, *et al.*, 2010. Third metacarpal condylar fatigue fractures in equine athletes occur within previously modelled subchondral bone. *Bone* **47**(4), 826–831. doi:10.1016/j.bone.2010.07.019

65. Shaffer SK, Stover SM, Fyhrie DP, 2023. Training drives turnover rates in racehorse proximal sesamoid bones. *Sci. Rep.* **13**(205), 1–12. doi:10.1038/s41598-022-26027-y

66. Nunamaker DM, Butterweck DM, Provost MT, 1990. Fatigue fractures in thoroughbred racehorses: Relationships with age, peak bone strain, and training. *Journal of Orthopaedic Research* **8**(4), 604–611. doi:10.1002/jor.1100080417

67. Hernandez J, Hawkins DL, Scollay MC, 2001. Race-start characteristics and risk of catastrophic musculoskeletal injury in Thoroughbred racehorses. *Journal of the American Veterinary Medical Association* **218**(1), 83–86. doi:10.2460/javma.2001.218.83

68. Wong ASM, Morrice-West AV, Whitton RC, Hitchens PL, 2023. Changes in Thoroughbred speed and stride characteristics over successive race starts and their association with musculoskeletal injury. *Equine Vet. J.* **55**(2), 194–204. doi:10.1111/evj.13581

69. Logan AA, Nielsen BD, 2021. Training young horses: The science behind the benefits. *Animals* **11**(2), 463. doi:10.3390/ani11020463

70. Malekipour F, Hitchens PL, Whitton RC, Vee-Sin Lee P, 2022. Effects of in vivo fatigue-induced microdamage on local subchondral bone strains. *J. Mech. Behav. Biomed. Mater.* **136**, 105491. doi:10.1016/j.jmbbm.2022.105491

71. Shaktivesh S, Malekipour F, Whitton RC, Lee PVS, 2024. Mechanical response of local regions of subchondral bone under physiological loading conditions. *J. Mech. Behav. Biomed. Mater.* **152**, 106405. doi:10.1016/j.jmbbm.2024.106405

72. Koshyk A, *et al.*, 2024. Influence of microarchitecture on stressed volume and mechanical fatigue behaviour of equine subchondral bone. *Bone* **182**, 117054. doi:10.1016/j.bone.2024.117054

73. Bergstrom TC, Spriet M, Carpenter RS, Jacques KL, Stover SM, 2025. Condylar fracture location is correlated to exercise history in Thoroughbred racehorses. *Equine Veterinary Journal* **57**(1), 76–86. doi:10.1111/evj.14091

74. Dempster DW, Birchman R, Xu R, Lindsay R, Shen V, 1995. Temporal changes in cancellous bone structure of rats immediately after ovariectomy. *Bone* **16**(1), 157–161. doi:10.1016/8756-3282(95)80027-N

75. Sims NA, Morris HA, Moore RJ, Durbridge TC, 1996. Increased bone resorption precedes increased bone formation in the ovariectomized rat. *Calcif. Tissue Int.* **59**(2), 121–127. doi:10.1007/s002239900098

76. Lerebours C, Buenzli PR, 2016. Towards a cell-based mechanostat theory of bone: the need to account for osteocyte desensitisation and osteocyte replacement. *J. Biomech.* **49**(13), 2600–2606. doi:10.1016/j.jbiomech.2016.05.012

77. Levenston ME, Beaupré GS, Jacobs CR, Carter DR, 1994. The role of loading memory in bone adaptation simulations. *Bone* **15**(2), 177–186. doi:10.1016/8756-3282(94)90705-6

78. Graham JM, Ayati BP, Holstein SA, Martin JA, 2013. The role of osteocytes in targeted bone remodeling: A mathematical model. *PLoS One* **8**(5), e63884. doi:10.1371/journal.pone.0063884

79. Turner CH, 1998. Three rules for bone adaptation to mechanical stimuli. *Bone* **23**(5), 399–407. doi:10.1016/S8756-3282(98)00118-5